CeOx/TiO2 (Rutile) Nanocomposites for the Low-Temperature Dehydrogenation of Ethanol to Acetaldehyde: A Diffuse Reflectance Infrared Fourier Transform Spectroscopy-Mass Spectrometry Study

CeOx/TiO2(Rutile) Nanocomposites for the Low-Temperature Dehydrogenation of Ethanol to Acetaldehyde: A Diffuse Reflectance Infrared Fourier Transform Spectroscopy–Mass Spectrometry Study

J. Velasquez Ochoa[a,*], E. Farci[a], F. Cavani[a],

F. Sinisi,[b] L. Artiglia,[b] S. Agnoli,[b] G. Granozzi[b]

M. C. Paganini[c]

L. Malfatti[d]

[a] Dipartimento di Chimica Industriale "Toso Montanari", Università di Bologna, Viale Risorgimento 4, 40136 Bologna (Italy)

[b] Dipartimento di Scienze Chimiche Università di Padova Via F. Marzolo 1 35131 Padova (Italy)

[c] Dipartimento di Chimica, Università di Torino, Via P. Giuria, Torino 10125, Italy

[d] Laboratorio di Scienza dei Materiali e Nanotecnologie, CR-INSTM, Dipartimento di Chimica e Farmacia, Università di Sassari, CR-INSTM, Via Vienna 2, 07100 Sassari, Italy

Abstract

Two nanocomposites of different layer thickness were synthesized by impregnation of a rutile titania support with a reduced ceria solution. An *in situ* spectroscopic DRIFTS-MS study has shown remarkable differences in the interaction of these nanocomposites with ethanol depending on the layer thickness and the environment (oxidizing/reducing). Under anaerobic conditions it was found that the surface-support interaction allowed to stabilize the ceria in the reduced form (Ce^{3+}) until temperatures as high as 300°C, especially for the thinner layer. The intrinsic characteristics of these materials were proven useful in the dehydrogenation of ethanol to acetaldehyde since they inhibited further oxidation products (typical in the case of bulk ceria) and dehydration products (such as ethylene, the main product for bulk titania), and even promoted aldolic condensation to crotonaldehyde. All this, without the need of using expensive noble metals as catalysts or hydrogen to keep the ceria reduced.

1. Introduction

Ceria-based nanomaterials have received a great deal of attention in the last decades owing to their physical and chemical properties, which are markedly different from those of the bulk materials. Due to their electronic conductivity and oxygen storage capacity, these materials have been proven useful as catalysts for soot oxidation, reforming, partial oxidation, and water–gas shift reaction.[1] Other energy-related uses are in the fuel cell technology or in the thermochemical water splitting.[1,2] The high oxidative capability and oxygen storage capacity of ceria is mainly associated with the low energy cost for oxygen vacancy formation and low redox potential between Ce^{3+} and Ce^{4+} cations, which allows an easy shift from one to the other depending on the environmental conditions. In addition to their well-known redox properties, their acid–base behaviour is

another interesting aspect of ceria-based catalysts. In general, ceria possesses highly basic surface O^{2-} ions and weakly acid cerium ions.[3] However, when ceria is combined with other oxides may exhibit higher acidity/basicity than the pristine metal oxide.[4,5] All these degrees of freedom can direct the actual activity of ceria oxides toward specific catalytic pathways.

In this paper we address the ethanol oxidation reaction on ceria/titania nanocomposites. There are several methods to synthetize such nanocomposites. For instance, L. Artiglia et al. prepared TiO_2@CeO_2 core@shell nanostructures by coating a titania Degussa-P25 powders (anatase and rutile mixed phase) with an ultrathin ceria shell by consecutive impregnations, so that by choosing the number of cycles, the thickness of the outer ceria shell can be controlled with monolayer precision. Interestingly, in the ultrathin regime the interfacial hybridization between the 4f band of ceria and the O 2p band of TiO_2 leads to a strong stabilization of the 4f levels, favouring the formation of Ce^{3+} species.[6–8] As shown in the present work, when the support is pure anatase, the ceria does not form a homogeneous layer, but segregated clusters (see Figure S1). On the other hand, if the support is a pure rutile phase, an external ceria layer discontinuously covers the titania particles, leaving part of the titania support and ceria/titania edges exposed and free to interact with the reagents (new active sites).

The reactivity of ethanol toward bulk CeO_2 or TiO_2 have been investigated previously over a wide range of model and real catalytic surfaces.[9–15] These studies indicated that initially ethanol chemisorbs dissociatively to produce surface ethoxy and hydroxyl groups: the former are bonded to surface metal cations, while hydrogen ions are attached to surface oxygen anions. The ethoxy groups generally undergo dehydrogenation and dehydration to give acetaldehyde or ethylene, respectively, depending on acid/basic site density, bond energy, electronegativity difference, and the oxygen electronic polarisability of the oxides.[16] In general, a large metal cation–oxygen anion bond energy favors dehydration over dehydrogenation as in the case of TiO_2, which has been shown to produce large amounts of ethylene as compared to acetaldehyde. On the other hand, a high basic site number, a small metal cation–oxygen anion bond energy and a high oxygen electronic polarisability favor dehydrogenation rather than dehydration and this is the case for the CeO_2. However, due to the intrinsic oxidative character of CeO_2, the formed acetaldehyde is further oxidized to acetates, acetone and even CO_2 and water (total oxidation).

This paper shows that when the ceria is deposited as a thin layer over the rutile support, the semi-shell formed exploits some good characteristic of both oxides (synergic effect) and allows to obtain a better selectivity to acetaldehyde without further oxidizing it. In fact, the possibility of tuning the redox and the acid base properties at the same time is important in order to develop more selective oxidation catalysts without the need of using expensive noble metals (Pd, Pt, Rh), toxic transition metals (Ni, Co) and hydrogen reductive pretreatments, for instance for ethanol steam reforming. [17–21]

2. Results and discussion

2.1. Characterization

Figure 1 shows the XRD diffraction pattern of the TiO_2 obtained by controlled hydrolysis of a $TiCl_4$ solution at low temperature (40°C) and two impregnated ceria/titania samples, labelled **TCR1**, and **TCR3** referring to composite nanostructures obtained after one or three impregnations of the rutile powder with a solution 0.45 M of Ce(III)-ethylhexanoate in hexane (to avoid Ce oxidation). After each impregnation, the powders were calcined at 650°C (see the Materials and methods section for details). For both the pure rutile TiO_2 sample and the mixed ceria/titania samples, the XRD showed only the diffraction peaks of the rutile, without any crystalline phase associated to Ce. The XRD pattern of bulk CeO_2 is included as reference.

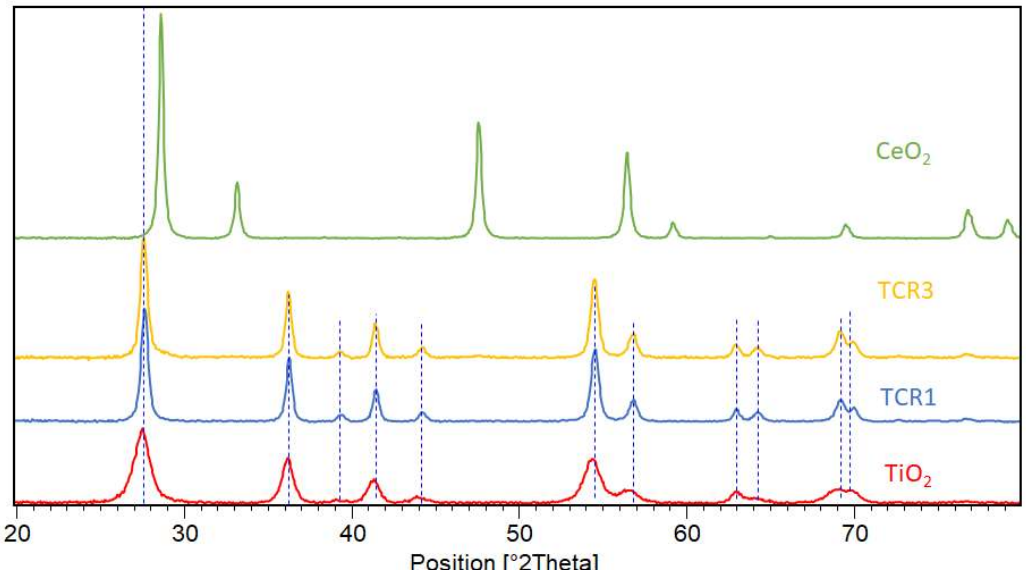

Figure 1. X-ray diffraction pattern for the synthesized TiO_2, TCR1, TCR-3 samples and a commercial CeO_2. Discontinues lines indicate the Rutile phase diffraction lines (PDF 98-004-1086).

The HR-TEM images of TiO_2 rutile phase after three successive ceria depositions with the Ce precursor solution (TCR3) show that the support particles are surrounded by a thin, but rough shell of about 1-2 nm of amorphous material (CeO_x) (Figure 2). However, from the analysis of several images, we have found that the rutile exposed surfaces are not necessarily fully covered by the CeO_x layer. It seems that the decoration of TiO_2 is not correlated to specific crystallographic orientation: the CeO_x layer can be observed on the {110} {001} or {101} surfaces of TiO_2, but sometimes the complete coverage is not obtained. This likely suggests that defects and kinetics phenomena strongly influence the growth. Similar results were obtained also for the TiO_2 powder after one impregnation cycle (TCR1), however in this case due to the low coverage and thinner thickness of the shell, it was very hard to identify unambiguously the ceria features. (Figure S2)

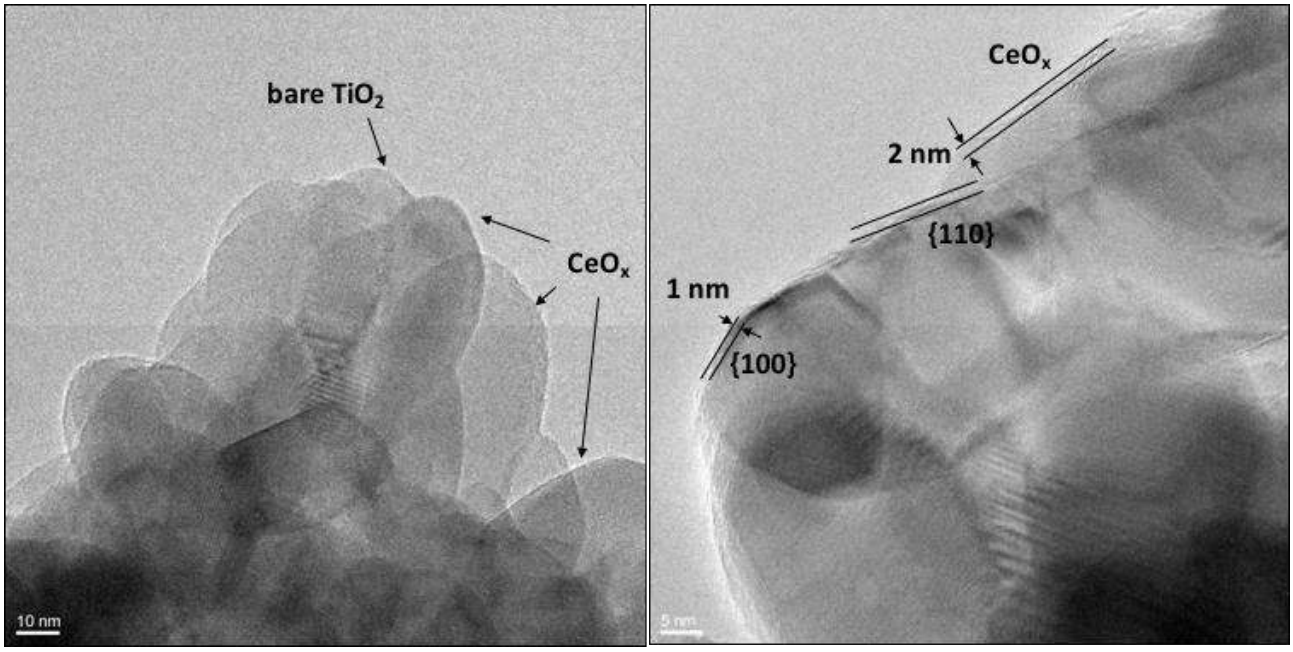

Figure 2. HR-TEM for the TCR3 sample using rutile-phase titania powders indicating the formation of an un-complete layer of CeO_x.

The Raman spectra of TCR1 and TCR-3 reported in Figure 3 confirm the rutile structure of the samples: the characteristic peak of ceria (at 463 cm^{-1}) is not observed. This suggests that in these samples the pristine Ce^{3+} ions are not oxidized to Ce^{4+}. On the other hand, since Raman spectroscopy is scarcely surface sensitive to the monolayer nanostructures, a more conclusive evidence for the unique presence of Ce^{3+} ions is provided by X-ray photoemission spectroscopy (XPS), see data below.

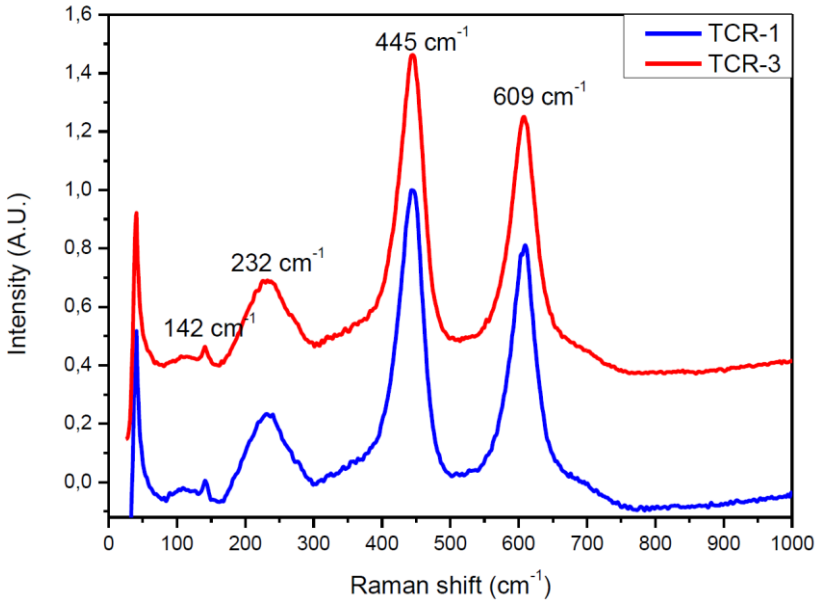

Figure 3. Raman spectra of the TCR1 and TCR-3 sample.

The specific surface areas and surface chemical composition of the investigated samples were then obtained by N_2 BET and XPS, respectively. The results (Table 1) show that the surface area of the mixed samples is slightly higher, even though within the experimental error, than that of the bare TiO_2 rutile. The XPS analysis reveals that the Ce/Ti ratio for the TCR-3 sample is three times that of the TCR1, demonstrating the linearity of the sequential impregnation procedure. No significant change is observed on going from pure TiO_2 to TCR1 and TCR-3 samples when observing the Ti 2p XPS peak. The Ce 3d photoemission line is reported in figure 4 and demonstrates the massive presence of Ce^{3+}. The spectra have been fitted using two doublets for the Ce^{3+} species and three doublets for the Ce^{4+} features, following a well-established procedure, [22] in order to take into account final and atomic multiplet effects. In the case of the TCR1 sample the cerium speciation is 90.0% Ce^{3+} and 10.0% Ce^{4+}, whereas in the TCR-3 powder Ce^{3+} 81.4 % and Ce^{4+} 18.6%. The strong stabilization of the Ce^{3+} species at the very interface with the TiO_2 support has been largely reported in the literature and was theoretically explained by Graciani et al. as deriving from the interfacial hybridization between the O 2p band of titania and the 4f levels of ceria.[23]

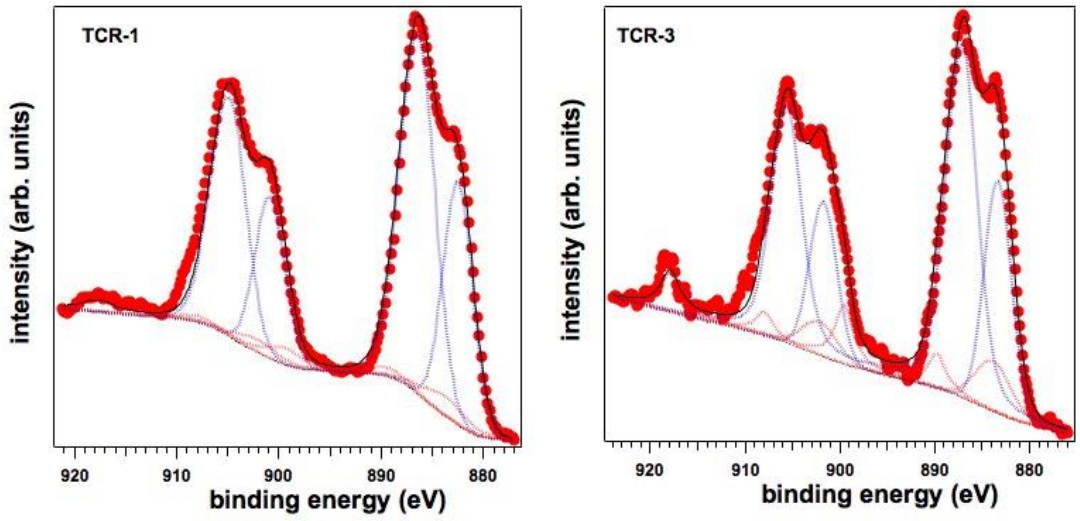

Figure 4. Ce 3d photoemission spectra and their deconvolution into chemically shifted components for TCR1 (left) and TCR-3 (right) samples. The blue dotted peaks are ascribed to Ce^{3+}, whereas the red dotted doublets to Ce^{4+}.

Table 1. Surface area and XPS results for the ceria, titania and mixed TCR samples

Catalysts	*Surface area $m^2 g^{-1}$*	*Ce/Ti [a]*
TiO_2 Rutile	17	--
Ceria	43	--
TCR1	25	0.06
TCR-3	23	0.18

2.3. In-situ DRIFTS-MS study of Ethanol adsorption

In this study ethanol was chosen as a probe molecule to elucidate the role of the TiO_2 exposed surface, the Ce layer thickness, and CeO_x/TiO_2 synergic effects on the catalytic properties of the nanocomposites (dehydration, dehydrogenation, oxidation). Moreover, the spectroscopic in-situ studies were performed both in presence and absence of oxygen to get an insight into the redox properties.

2.3.1. Anaerobic oxidation (In He):

Ethanol was sent as a pulse and adsorbed at room temperature over each sample: the TCR1 and TCR3 nano-composites and the bare TiO_2 and CeO_2 powders. Afterwards, the carrier gas (He) was let to flow in order to remove the alcohol physically adsorbed. Later on, the temperature was raised at a constant rate of 10°C min^{-1} and spectra at different temperatures were registered. The results presented in the following figures are those after subtraction of the catalyst spectrum previously recorded at each temperature.

Figure 5a presents the comparison of the spectra at room temperature (30°C) after an ethanol pulse. It was observed that the spectra of the mixed samples and of bare TiO_2 are similar. On them, the ethanol molecule adsorbs molecularly and dissociatively as an ethoxy group (eqn (1) and eqn (2)).[10,12,24] In fact, the bands at 1380 and 1478 cm^{-1} ascribed to $\delta_s(CH_3)$ and $\delta_{as}(CH_2)$ of the adsorbed alcohol together with the broad band at 3200 cm^{-1} for the OH stretching are the most intense. Besides, the spectra shows a series of features at 1125, 2972, 2930 and 2872 $cm^{-1,}$ which are the characteristic bands associated with $\nu_{as}(CO)$, $\nu_a(CH_3)$, $\nu_a(CH_2)$ and $\nu_s(CH_3)$ of ethoxy species.[25] The ceria sample on the other hand, apart from the bands for ethoxy and ethanol (including the C-C and C-O stretching at 1063, 1105 and 1123 cm^{-1}, which were not sufficiently intense to be observed one the TiO_2) presented additional bands that were already ascribed in the literature to acetate species (See Equation 6) upon the adsorption of ethanol on fully oxidized CeO_2 (1312, 1445, 1561 and 2840 cm^{-1} corresponding to $\delta_s(CH_3)$, $\nu_s(OCO)$, $\nu_{as}(OCO)$ and $\nu_s(CH_3)$ respectively) [11,26] as well as bands at 885 and 903 cm^{-1} that correspond to new Ce^{4+}-O (O from ethanol) interactions. Thus, in the case of the mixed samples, TCR1 and TCR-3, the absence of the acetates and Ce^{4+}-O bands confirms that the ceria present is being stabilized as Ce^{3+} at this temperature in both samples.

A similar phenomena (absence of acetates in the IR spectra) was observed by Idriss and co-workers [10] using Au deposited on CeO_2, from there it was concluded that Au had an effect on the reduction of the surface of CeO_2 (confirmed by Ce 3d photoemission spectra). More in general, the adsorption of ethanol on H_2-reduced M/CeO_2 was thoroughly studied confirming the absence of acetate species when surface oxygen species are depleted.[13,27] Moreover, it is stated that the partial reduction of the oxide support caused by the addition of a noble metal (creation of oxygen vacancies) inhibits the oxidation pathways. However, it is important to notice

that in our case, neither the hydrogen nor a noble metal is required to keep the Ce reduced and thus to inhibit oxidation, but it is the interfacial hybridization with the support that stabilized ceria in a low oxidation state. For all samples, the spectra at 30°C exhibit a negative peak at ca 3679 cm^{-1} that is attributed to the loss of surface free OH groups when they bind to the alcohol and desorb as water (See eq. 2).[28,29] In fact, another negative band observed at 1631 cm^{-1} is related to the bending of water that is desorbed. In the case of pure TiO_2, the desorption of water is less and instead, newly formed OH surface groups produce the band at around 3407 cm^{-1}. This can indicate that in this case, OH groups remained on the surface, being produced by the ethanol dissociation as in Equation 3.

Table 2. Surface reactions observed during the Ethanol desorption experiments

Equation	***Reaction***	***Description***
(Eq. 1)	$C_2H_5OH_{(g)} \rightarrow C_2H_5OH_{(a)}$	Adsorption of molecular ethanol
(Eq. 2)	$C_2H_5OH_{(a)} + OH_{(s)} \rightarrow C_2H_5O^-_{(a)} + H_2O_{(g)}$	Ethoxy groups formation and water desorption
(Eq. 3)	$C_2H_5OH_{(a)} + O_{(s)} \rightarrow C_2H_5O^-_{(a)} + OH_{(s)}$	Ethoxy groups formation without water desorption
(Eq. 4)	$C_2H_5O^-_{(a)} \rightarrow CH_2CH_{2(g)} + H_2O_{(g)}$	Ethylene formation (dehydration)
(Eq. 5)	$C_2H_5O^-_{(a)} + OH_{(s)} \rightarrow CH_3CHO_{(g)} + H_2O_{(g)}$	Acetaldehyde formation (further dehydrogenation of ethoxy groups)
(Eq. 6)	$CH_3CHO_{(g)} + O_{(s)} \rightarrow CH_3COO^-_{(a)} + H_{(a)}$	Acetates formation, observed in CeO_2 at low temperature and on the other samples only at high temp.
(Eq. 7)	$2CH_3COO^-_{(a)} \rightarrow CH_3C(O)CH_3 + 2O^{2-}_{(s)}$	Acetone formation
(Eq. 8)	$CH_3COO^-_{(a)}OH_{(s)} \rightarrow CH_4 + CO_3^{2-}$	Carbonates formation
(Eq. 9)	$2CH_3CHO_{(g)} \rightarrow CH_3CH = CHCHO + H_{(a)}$	Crotonaldehyde formation
(Eq. 10)	$C_xH_y + N(O_2) \rightarrow x(CO_2) + \frac{y}{2}(H_2O)$	Complete oxidation *

(a) for adsorbed; (s) for surface; (g) gas phase.* x refers to the number of carbon atoms in the hydrocarbon, y refers to the number of hydrogen atoms and N refers to the number of oxygen atoms required in the hydrocarbon combustion reaction.

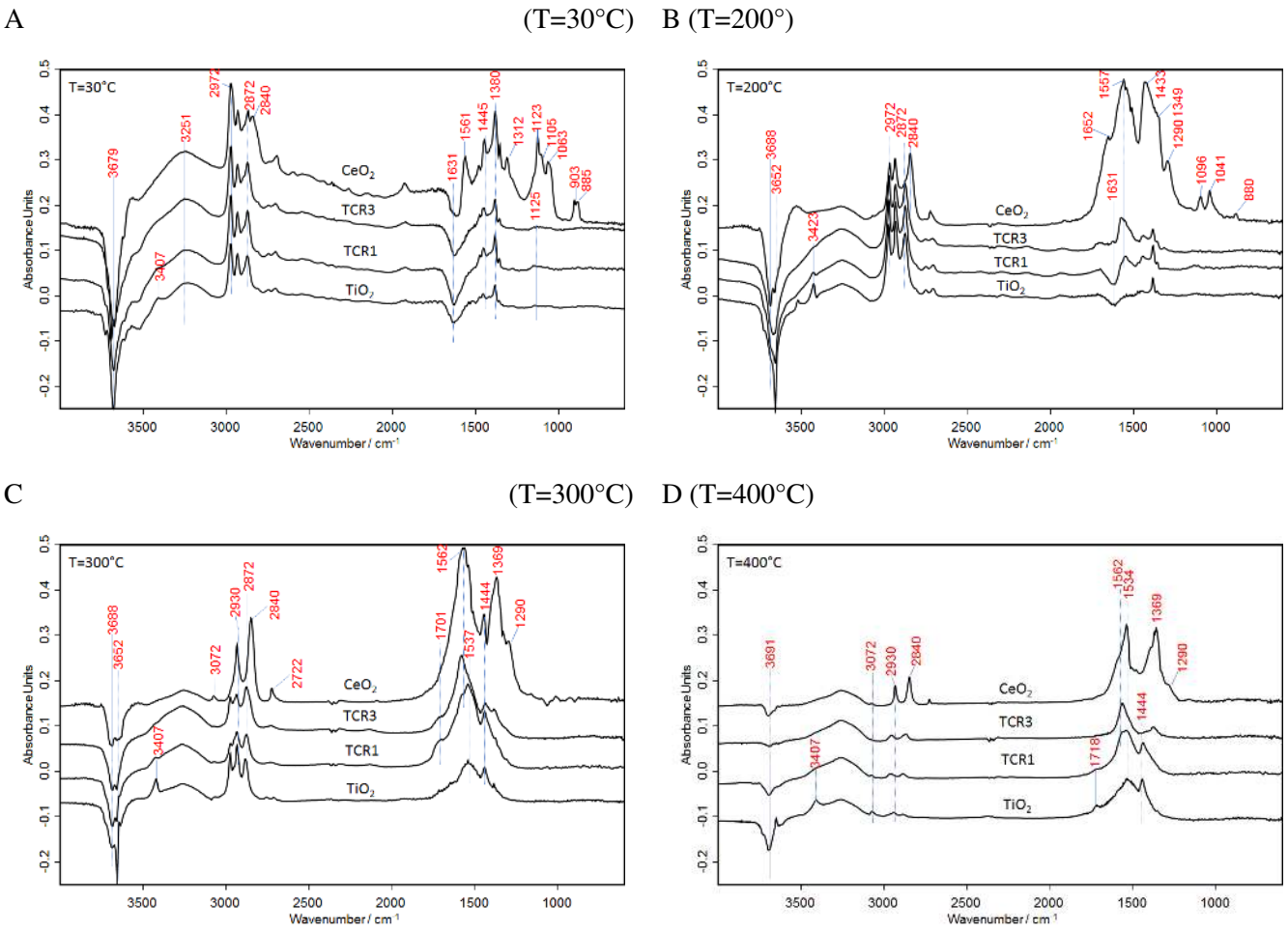

Figure 5. DRIFT spectra during Ethanol TPD in He (anaerobic) for the ceria, titania and mixed TCR samples.

The comparison of spectra for the samples after heating at 50 and 100°C (not shown) did not present significant changes with respect to those recorded at 30°C. Instead, when the temperature reaches 200°C (Figure 5b) the intensity of the acetate bands for the ceria increased considerably, and new band at 1653 cm^{-1} appeared indicating the presence of a C=O stretching, probably due to a further oxidation of the acetates to acetone that has been already reported in literature [9] (See equation 7). Conversely, for the titania and the mixed samples, the prevailing bands at this temperature are still those of ethanol (including the negative band at 1631 cm^{-1}) and only a small band at 1572 cm^{-1} (TCR3) could indicate the formation of acetates. The acetate bands are observed on Titania only at higher temperature or after an oxidizing pretreatment (see data below), thus we can deduce that for the mixed samples a synergic effect is active in which the CeO_x layer donates oxygen to the titania allowing the low temperature formation of acetates.

At 300°C, acetate bands were present as well in all samples, although shifted toward higher wavenumbers for TCR-3, and to lower wavenumbers for both TC1-R and titania, indicating a different strength in the two cases. A band at 1701 cm^{-1} appeared for the mixed samples (more evident for the TCR1), which is attributable to a C=O stretching of crotonaldehyde together with another band at 1581 cm^{-1} that is partially covered by the acetate bands, but easily observed during the fitting (See Figure S3). These bands have been observed in the

literature and attributed to crotonaldehyde adsorbed directly on TiO_2 polymorphs.[30] At 400°C, evidence of the transformation of acetate species to carbonate was shown for CeO_2, since the intensity of band at 1562 cm^{-1} decreased, while a new band was formed at 1534 cm^{-1}. This band, together with that at 1369 cm^{-1} have been attributed in the literature to bidentate carbonates.[11] The bands falls at the same wavelength for TCR-3, whereas in the case of TCR1 and Titania the band positions are still those of acetates. Table 2 summarizes the surface reactions observed during the experiments.

In general, these spectra show that especially at low temperature, the Ce present in TCR samples is stabilized as Ce^{3+} since the TCR samples did not present the typical acetate and carbonate bands associated with the oxidized Ce.

The products desorbed during this Ethanol-TPD experiments were monitored on-line with a mass spectrometer. The results (Figure 6) showed that the TC1R has increased dehydrogenating properties, being able to produce acetaldehyde at lower temperature and with relatively higher intensity. This phenomenon can be explained because even though ceria is mostly reduced in both samples, in the case of the TCR3 (81.4% Ce^{3+}), the outer film and therefore that in real contact with the gas phase, presents mainly Ce(IV). On the other hand, the TCR1 (90% Ce^{3+}) has more Ce^{3+}-Ti interface available that has been claimed to have a particular enhanced activity in the production of formaldehyde from methanol.[23] Another observation is a higher relative amount of crotonaldehyde in the temperature range confirming that this sample has also the ability to condensate the acetaldehyde molecules produced, thus settling the spectroscopic DRIFT results.

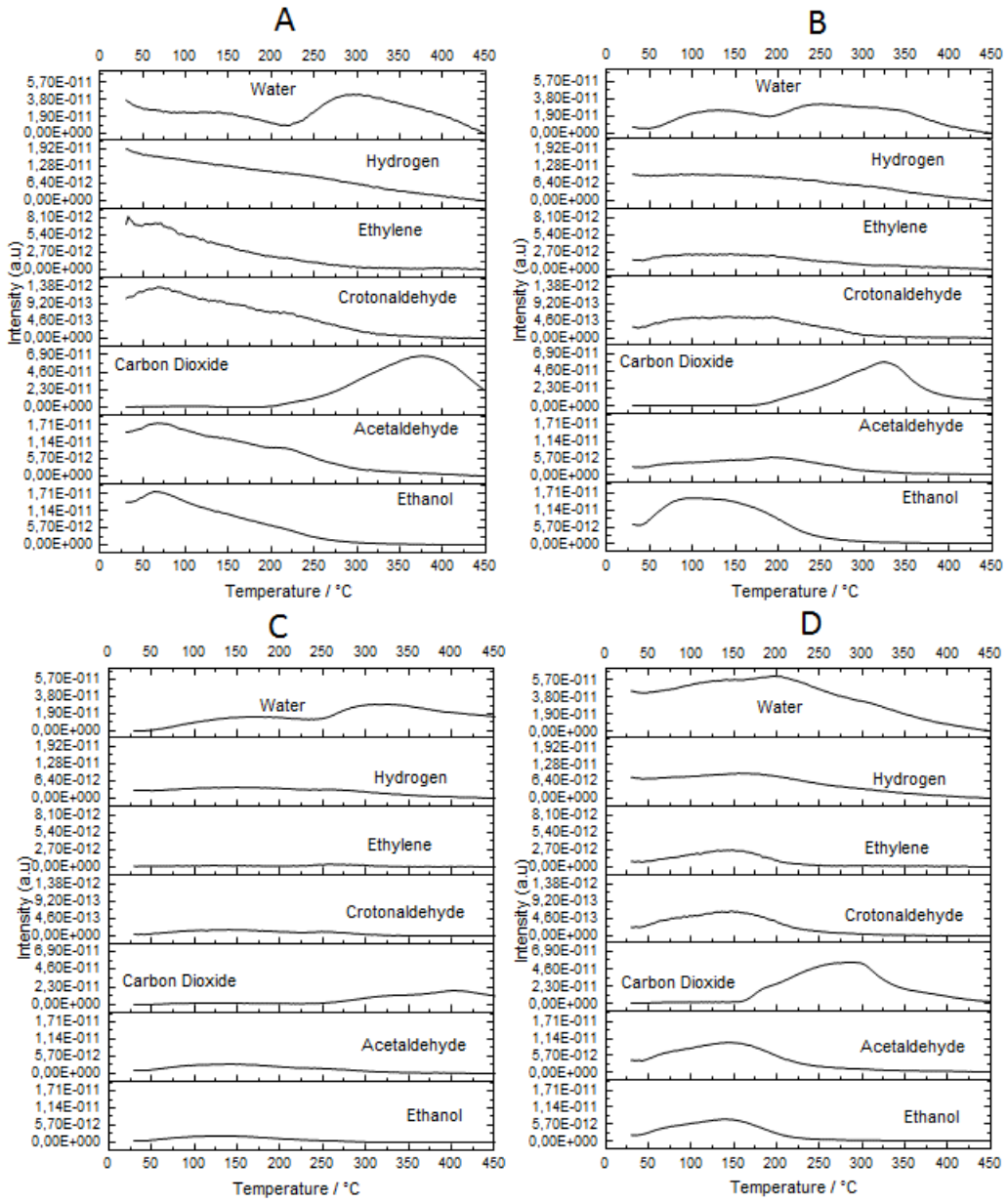

3

Figure 6. Main products monitored during ethanol TPD in He for the samples TC1-R (A) TC3-R (B), TiO_2 (C) and CeO_2 (D) on ceria, titania and TCR mixed samples

In overall, this result allows to deduce the pathway preferentially followed by ethanol adsorbed either on the pure oxidized CeO_2 or in the mixed oxides (stabilized Ce^{3+}) when there is no additional oxygen in the environment (Figure 7). Initially ethanol is adsorbed molecularly or dissociated as an ethoxy group. Then, the ethoxy groups undergo dehydrogenation yielding acetaldehyde. The residual hydrogen from ethanol adsorption might desorbs either as H_2O or as H_2 depending on the surface characteristics. Usually, surfaces that promote oxidative dehydrogenation reactions (that releases water) are those containing reducible and reoxidisable cations as in this case (whereas on clean metals such as Ni, Pt and Pd, ethanol is dissociated to ethoxy groups and adsorbed hydrogen).[13] The formed acetaldehyde can be further oxidized to acetates as in the case of Ce^{4+} or to undergo an aldolic condensation to crotonaldehyde as in the case of the mixed TC-R

samples at low or mild temperature. When the temperature increases, the Ceria donates some oxygen to the titania in the case of the mixed samples, and the formed intermediates are also oxidized.

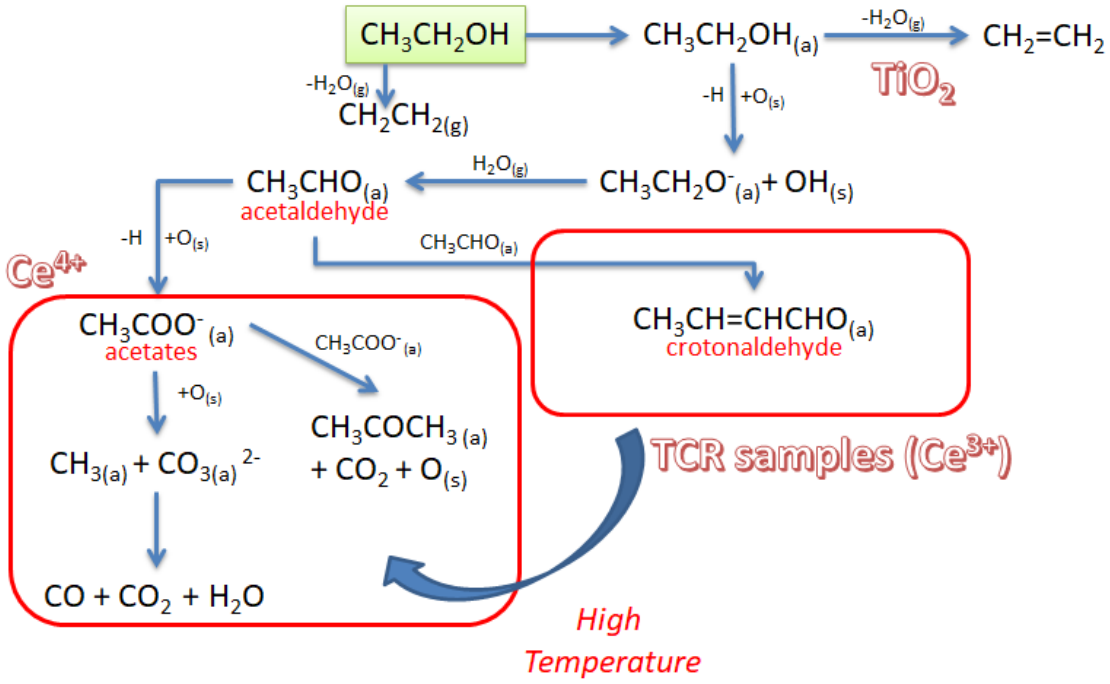

Figure 7. Surface pathways followed by the ethanol adsorbed on the single (CeO_2) or the mixed oxides (stabilized Ce^{3+}) under anaerobic conditions.

2.3.2. Oxidizing pretreatment

The same study was performed using samples previously exposed to an oxidizing environment (450°C for 20 min in air). DRIFTS results presented in Figure 8 show that in this case the mixed samples present an adsorption spectrum different from that of titania and ceria since also the TiO_2 shows the typical acetate bands even at low temperature, instead, the TCR1 and TCR-3 samples start showing these signals at higher temperatures (200°C for the TCR-3 and 300°C for the TCR1). This effect clearly shows the stabilization of the Ce^{3+} species on the mixed samples (especially in the sample impregnated only once) even after an oxidizing pretreatment. Interestingly, in the case of the mixed samples, the absorption bands in the region of 1650-1723 cm^{-1} (starting at 200°C for the TCR-3) might be an indication of the formation and adsorption of species such as acetaldehyde and crotonaldehyde that are not present in the single oxide samples. This confirms the improved dehydrogenation and condensation properties of these mixed nanocomposites.

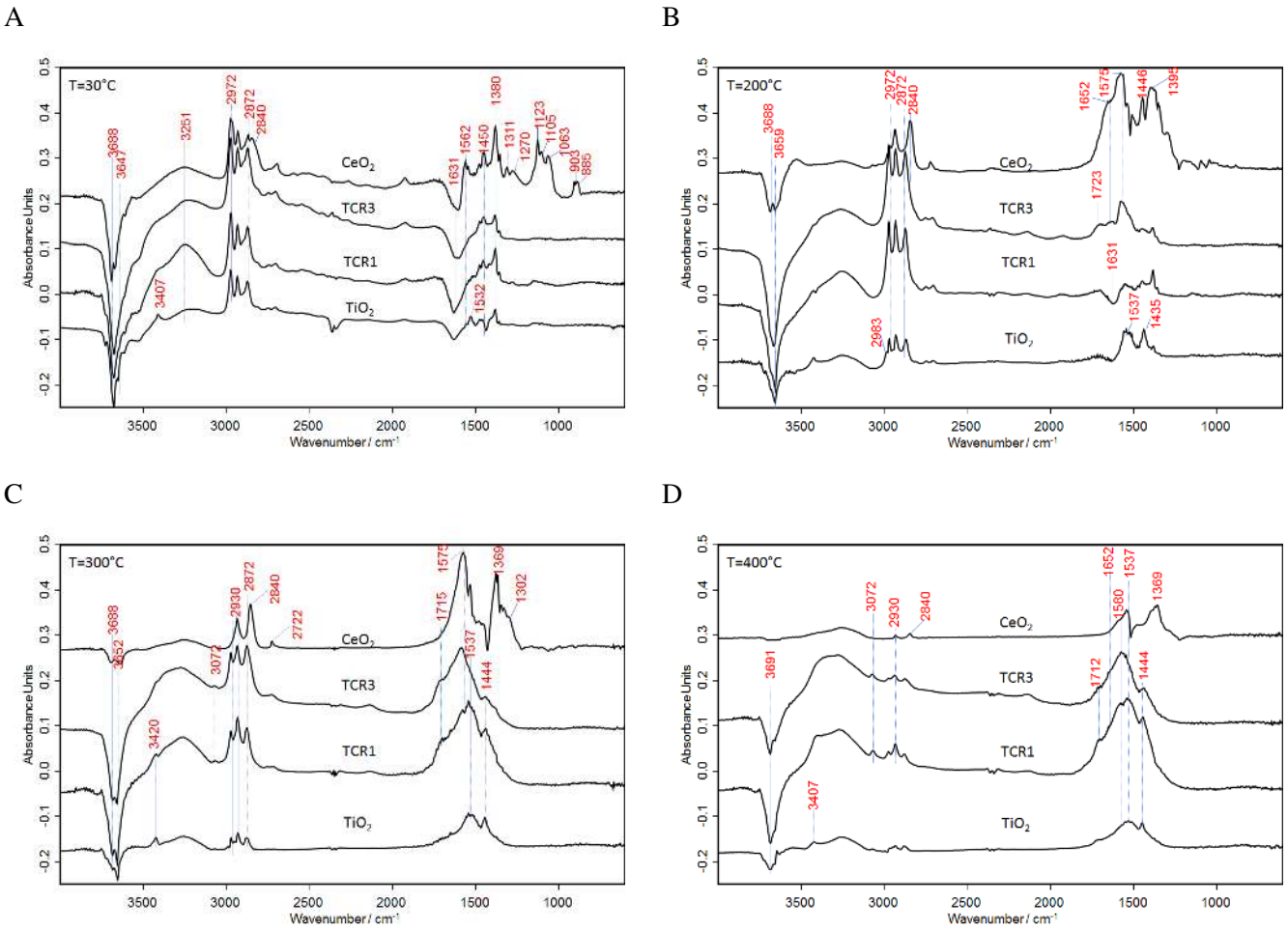

Figure 8. DRIFTS Spectra of Ethanol TPD at 30°, 200, 300 and 400 °C of the catalysts pretreated at 450°C in air.

The on-line MS measurements during these experiments (Figure 9) confirm that after the oxidizing pretreatment the Ceria (and Titania in lower amounts) produces water and CO_2 starting from lower temperatures; the latter may be produced by the decomposition of surface carbonates, which on these samples is seen in the middle range temperature (200-300°C). On the other hand, the mixed samples have a higher dehydrogenating/dehydrating character at low temperature (producing acetaldehyde, crotonaldehyde and ethylene) and the total oxidation happens only at high temperatures.

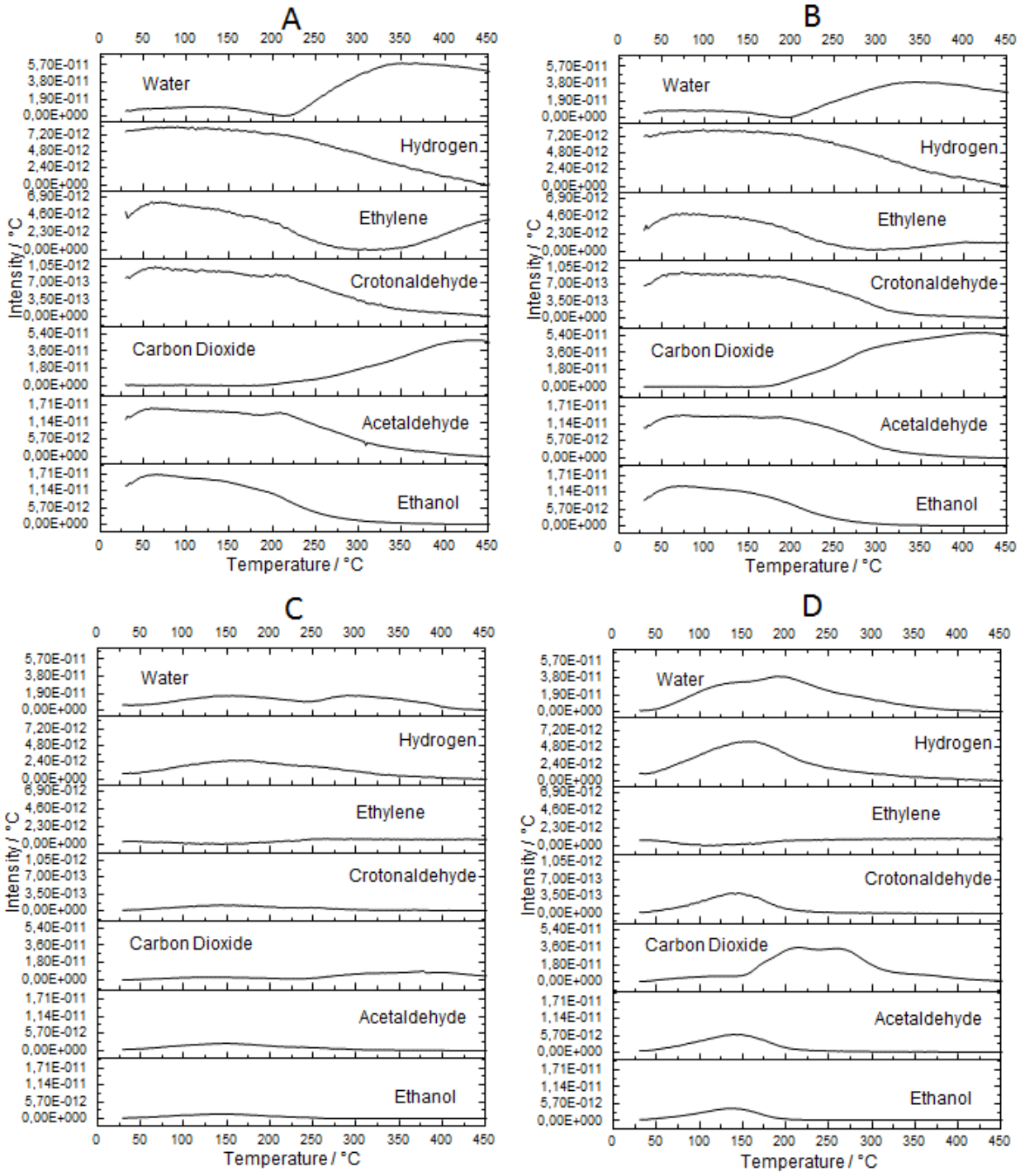

Figure 9. Main products monitored during ethanol TPD after oxidizing pretreatment for the samples TC1-R (A) TC3-R (B), TiO_2 (C) and CeO_2 (D) on ceria, titania and TCR mixed samples.

2.3.3. Aerobic Oxidation

Further in-situ DRIFTS studies were performed, but in this case the desorption of ethanol was done in a continuous flow of air. The spectra shown in Figure 10 reveal that under an oxidizing atmosphere the

stabilization effect of the Ce^{3+} is lost already at 200°C (since the acetate band at 1548 cm^{-1} is already intense, especially for TCR-3). Under these conditions, the intermediates are more easily desorbed probably due to a direct oxidation. In fact, there was no evidence of crotonaldehyde adsorbed on the surface for the mixed samples. At 300°C the surface is already clean for the CeO_2 sample whereas acetates and carbonates are present for the other samples. At 400°C only the TiO_2 still retains some adsorbed acetates. These tests confirm that the reduced Ce is needed if the goal is to promote dehydrogenation and condensation reactions.

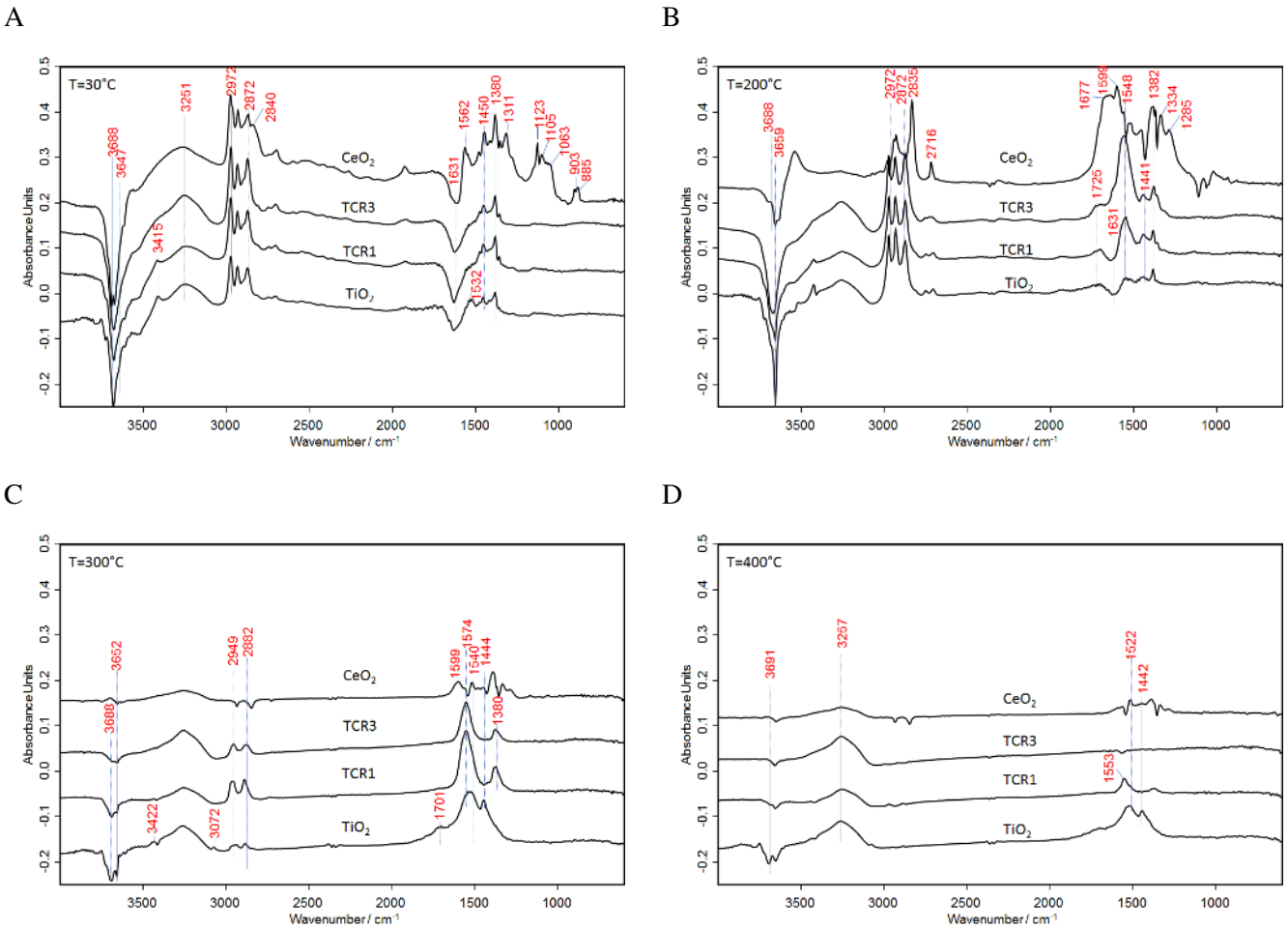

Figure 10. *DRIFT spectra during Ethanol TPD in air (aerobic) for the ceria, titania and mixed TCR samples.*

2.3.4. ***REACTIVITY TESTS***

In order to confirm the high selectivity of the TCR1 sample towards acetaldehyde, a catalytic test was performed using a continuous flow reactor, feeding ethanol at 15 mol.% either in N_2 or O_2 (total flow 30 mL min^{-1}). Downstream products were continuously monitored by an online Micro-GC and the results are presented in the following figures. The results confirm that in an oxidizing environment, the highest selectivity to acetaldehyde is achieved at medium - high temperatures, whereas anaerobic conditions favor a very high selectivity (>80%) at much lower temperatures (<250°C).

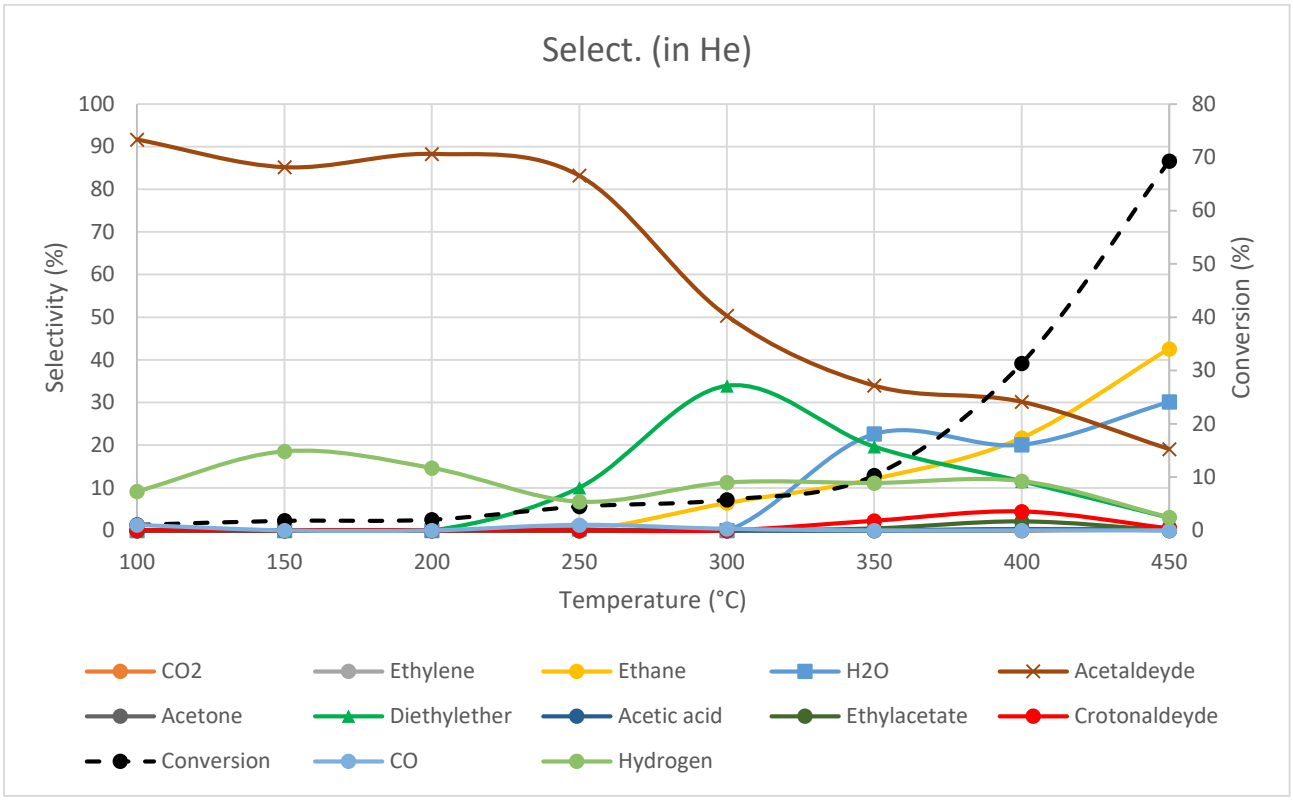
Select. (in He)
Selectivity (%)
Conversion (%)
Temperature (°C)
100
90
80
70
60
50
40
30
20
10
0
80
70
60
50
40
30
20
10
0
100
150
200
250
300
350
400
450
CO2
Ethylene
Ethane
H2O
Acetaldeyde
Acetone
Diethylether
Acetic acid
Ethylacetate
Crotonaldeyde
Conversion
CO
Hydrogen

A

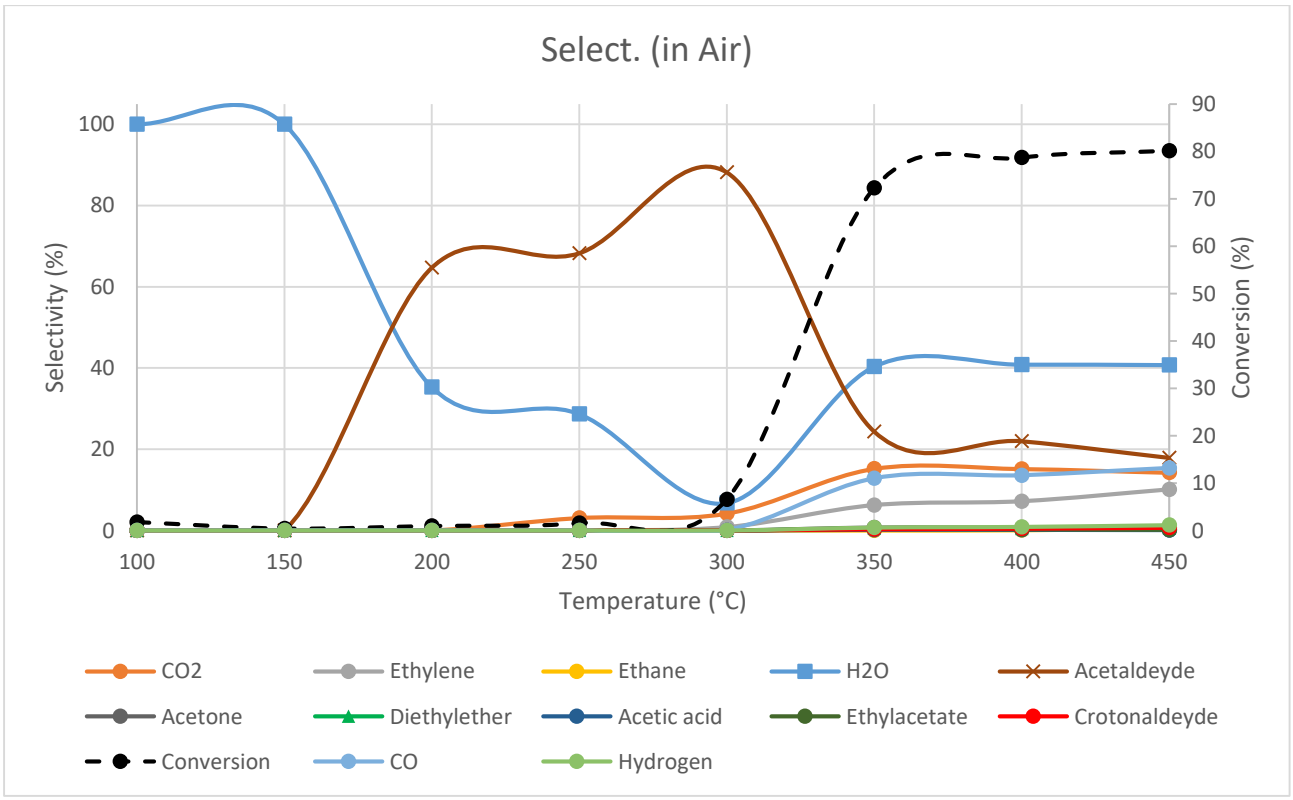
Select. (in Air)
Selectivity (%)
Conversion (%)
Temperature (°C)
100
80
60
40
20
0
90
80
70
60
50
40
30
20
10
0
100
150
200
250
300
350
400
450
CO2
Ethylene
Ethane
H2O
Acetaldeyde
Acetone
Diethylether
Acetic acid
Ethylacetate
Crotonaldeyde
Conversion
CO
Hydrogen

B

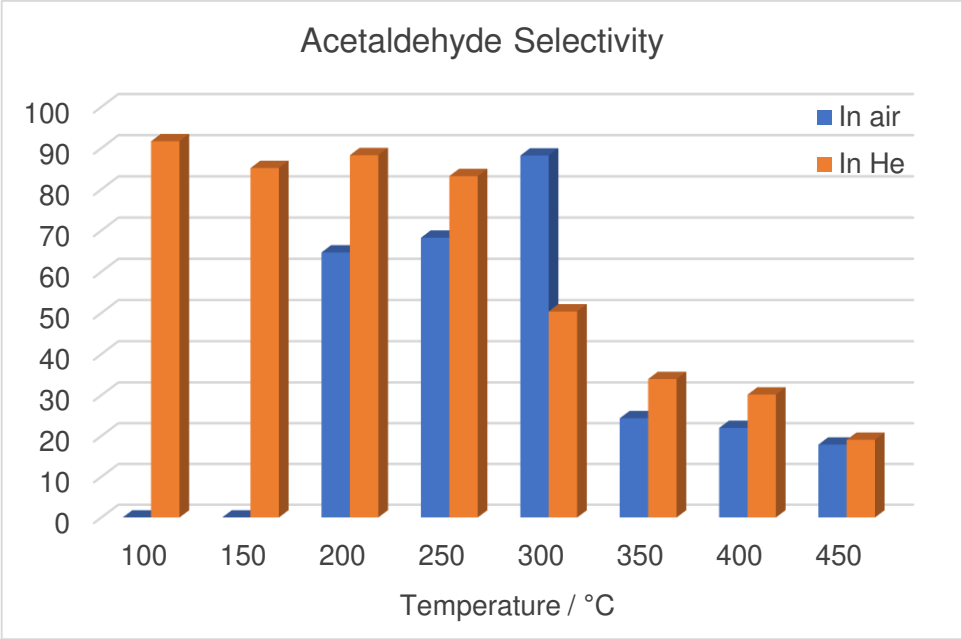

C

Figure 12. A) Catalytic performance for the TCR1 under anaerobic conditions. B) Catalytic performance for the TCR1 under aerobic conditions. C) Comparison on acetaldehyde selectivity for the TCR1 nanocomposite under anaerobic and aerobic conditions.

2.4. Pyridine Adsorption tests

Pyridine adsorption has been extensively used to characterize the acidity of solids. Figure 13 compares the spectra of pyridine adsorbed on TiO_2 rutile, CeO_2 and the mixed composites TCR1 and TCR3. The spectra were taken following pyridine adsorption and outgassing at 50°C taking the catalyst as background.

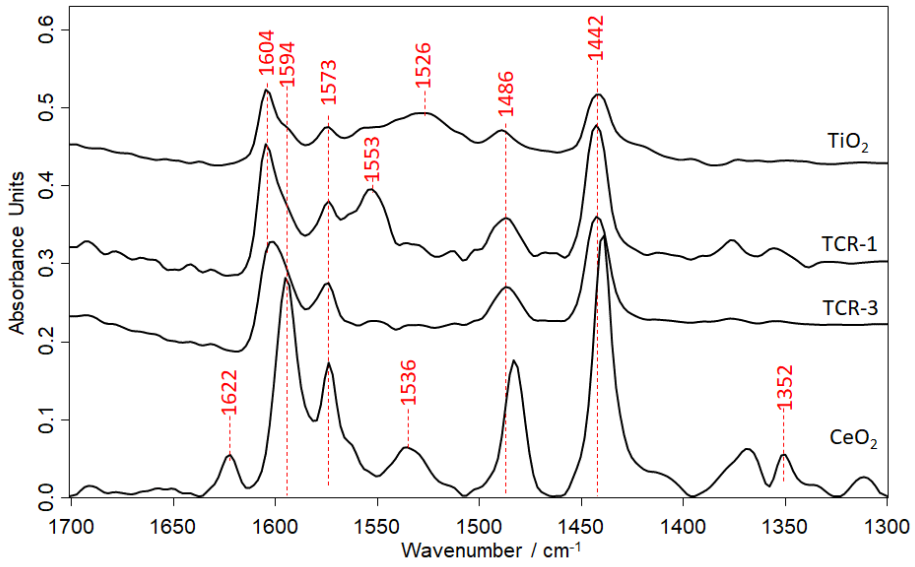

Figure 13. Comparison of DRIFTS spectra after pyridine adsorption and evacuation at 50°C for the CeO_2, TiO_2 and nanocomposites TCR1 and TCR3.

CeO_2 sample presented mainly Lewis acid sites (1439 and 1594 cm^{-1}) but also some Bronsted sites (at 1536 and 1622 cm^{-1}). On the TiO_2, the bands corresponding to Lewis acidity are found at 1604 an 1441 cm^{-1}, whereas the broad band at 1526 cm^{-1} has been assigned to a weaker Lewis interaction when pyridine is in excess.[31] These are findings in agreement with previous literature data indicating that Ti^{4+} is a stronger Lewis site compared with Ce^{4+}. [32,33]

In the case of the composites, the bands at 1604, and 1442 cm^{-1} can be assigned to the presence of Lewis sites, as for the TiO_2 whereas the band at 1486 cm^{-1} is assigned to H-bonded pyridine. Interestingly, the TCR1 sample presents a band at 1553 cm^{-1}, which is absent in the TCR-3 and only slightly visible on the TiO_2. This band is not directly related to Lewis or Bronsted acid sites. Instead, it has been observed to form after an oxidative break down of the adsorbed pyridine into carboxylate or carbonaceous surface species, which implies existence of considerably reactive basic sites (O^{2-}).[34] These sites might be responsible for the improved dehydrogenating and condensation properties of this sample.

Further evacuation of the pyridine at higher temperatures (Figure S4) showed that the samples containing Ti are endowed with stronger Lewis sites (that remain even at 400 °C), whereas in the case of the CeO_2 the spectrum at 200°C presents new bands including one at 1553 cm^{-1} observed in the TCR1 at low and middle temperature and attributed to a reactive basic site, which might be active in acetaldehyde and crotonaldehyde production. In fact, at this temperature these molecules start to be produced on the CeO_2, whereas on the TCR1 are produced before. Table 3 summarizes the assignment of the main bands for this probe molecule on our samples.

Table 3. Assignment of the pyridine bands observed for each catalyst

CeO_2	***TCR-3***	***TCR1***	***TiO_2***	***Assignment***
1439	1442	1442	1441	L-Py (19b)
1483	1486	1486	1486	L+B
			1526	L-Py (weak)
1536				B-Py (19b)
1553*		1553	1557*	Basic O^{2-} site
1574	1574	1573	1574	H-Py (8a)
1594	1601	1604	1604	L-Py (8a)
1622				B-Py (8a)

L-Py: Pyrydine coordinated to Lewis acid sites, B-Py: Protonated (Bronsted) pyridine, H-Py: H-Bonded pyridine. 8a and 19b is the notation of particular stretching modes of the pyridine adsorbed[35]. * refers to a band observed on these catalysts but at higher temperature than for the TCR1.

3. Conclusions

The addition of CeO_x to the TiO_2 rutile phase, do not yield a mixture of reactivity composed of both TiO_2 and CeO_2 oxides. Instead, it was found that this combination of materials gave a unique reactivity and selectivity with respect to its structure and relative chemical composition that holds no identifiable relation to either surface on its own. This synergistic effect is on the one hand directly connected to the interfacial hybridization between the two materials that helps to stabilize quite strongly the ceria in a reduced state and on the other hand to the peculiar nanoscale morphology of the composite that presents adjacent sites with quite diverse acid/base properties. In the mixed samples, the reduced ceria promotes ethanol dehydrogenation to acetaldehyde and avoids overoxidation. Moreover, it also favors the carbon–carbon bond formation and subsequent dehydration (to form crotonaldehyde) because they possess the Lewis acid and base sites required to bind the two aldehyde molecules and abstract the α-hydrogen. This special combination of redox and acid/base sites can be found on the nanocomposites at the interphase between the reduced ceria shell and the TiO_2 support.

This work exemplifies the great potential for catalysis of oxide/oxide interfaces which is in vogue these days:[36] by controlling at the nanoscale their structural properties (e.g. thickness and morphology) it is possible tailor their redox and acid/base chemistry in order to favor the desired reaction path. In this study, this type of chemistry was exploited to obtain a new sustainable and low-priced catalyst for the selective oxidation of ethanol to acetaldehyde at low temperature, without the need of using expensive noble metals (Pd, Pt, Rh), toxic transition metals (Ni, Co) and hydrogen reductive pretreatments.

Modello/Graphical abstract (da fare)

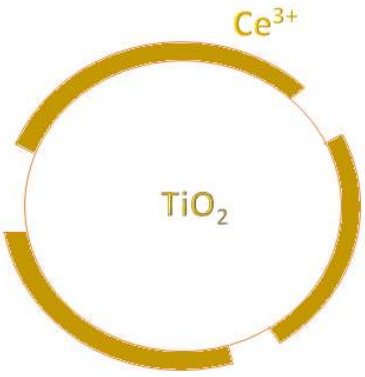

4. Materials and Methods

Synthesis of the TiO_2-CeOx (TCR) nanocomposites: The rutile-phase TiO_2 was obtained by controlled hydrolysis of a $TiCl_4$ solution (0.28 M) in deionized water at low temperature (40°C) during 3 days. The solid obtained was filtered and dried at 150°C for 24h and then thermally treated at 650°C for 2h to get the reference TiO_2 sample. The TiO_2-CeOx samples were obtained by impregnation of the TiO_2 powder (previously dried for 2h at 450°C) with a cerium (III) 2-ethylhexanoate solution 0.45 M. The mixture was stirred for 5 h; afterward, the powder was filtered and washed with n-hexane to remove any precursor residue. The product was dried and then calcined at 650 °C (heating ramp of 5 °C min^{-1}) in air for 8 h.

Characterization: ***XRD*** measurements were carried out using a Philips PW 1710 apparatus, with Cu Kα (λ = 1.5406 Å) as radiation source in the range of $5°<2\theta<80°$, with steps of 0.1 grade and acquiring the signal for 2 seconds for each step. ***BET*** single point analysis method was used to measure the surface area and it was carried out in a Carlo Erba Sorpty 1700 apparatus, using 0.5g of the sample pretreated at 150°C under vacuum (4 Pa).

XPS measurements have been carried out in a custom made VG Escalab MKII electron spectrometer. A water suspension of the powder samples was drop casted on a gold coated metal substrate obtaining thin films that were outgassed overnight before collecting the spectra. All measurements were carried out at room temperature using a non monochromated Al Kα source (Omicron DAR 400). Due to electrostatic charging, the binding energy scale was calibrated setting the adventitious carbon signal to 284.8 eV. The photoemission peak have been fit with Voigt functions after the subtraction of a Shirley background.

The Raman spectra were collected using a ThermoFisher DXR Raman microscope using a laser with an excitation wavelength of 532 nm (5 mW), focused on the sample with a 50 objective (Olympus).

A JEOL 3010-UHR Instrument (acceleration potential 300 kV, LaB6 filament) (JEOL Ltd., Milan, Italy) was utilized to acquire the High Resolution-Transmission Electron Microscopy (HR-TEM) images to evaluate the morphology of the described catalysts. For TEM analyses, the samples were deposited on a copper grid, coated with a porous carbon film; the digital micrographs were acquired by an Ultrascan 1000 camera and the images were processed by Gatan digital micrograph.

In-situ DRIFTS-MS: The undiluted powder sample is first thermally treated from 30 to 450°C in He flow (8 mL min^{-1}) and hold for 20 min. Then the sample is cooled down to room temperature (30°C) and Ethanol is fed (0,01 mL) vaporizing it with the help of a heated line that goes into the cell. Subsequently, He is left to flow until weakly adsorbed ethanol was evacuated. The temperature is raised until 450°C at 10°C min^{-1} registering the spectra (DRIFT and on-line MS) every 50°C. The following selected mass spectroscopy signals (m/z) are monitored continuously with time (and temperature): 2, 16, 25, 28, 29, 30, 31, 40, 41, 43, 44, 45, 56, 58, 59, 60, and 61. By combining the information obtained from several different m/z signals, it is possible to obtain

unambiguous information on the various products formed. The IR apparatus used is a Bruker Vertex 70 with a Pike DiffusIR cell attachment. Spectra are recorded using a MCT detector after 128 scans and 4 cm^{-1} resolution. The mass spectrometer is a GeneSys evolution from European Spectrometry Systems.

Catalytic tests: Reactivity experiments are carried out using 150 mg of catalyst in a continuous flow reactor, operating at atmospheric pressure. Ethanol percent is fixed to 15 mol.% in N_2 (total flow 30 mL min^{-1}). Downstream products are continuously monitored by an online Micro-GC using an Agilent-3000A instrument equipped with three columns (Plot-Q, OV1 and Molecular sieve 5A) and TCD detector.

Supplementary Information

Figure

Figure S1. For samples using the anatase polymorph after three consecutive impregnation cycles each followed by a thermal treatment, a uniform ceria layer is not observed but segregated crystalline CeO_2 clusters about 3-5 nm wide decorating the edges and the corners of the anatase nanoparticles.

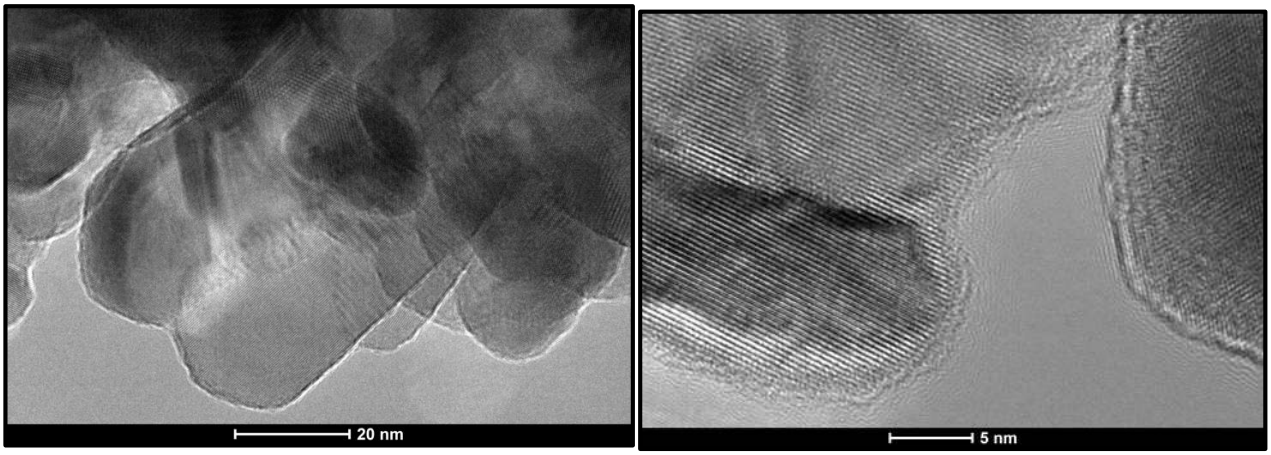

Figure S2. TEM images showing a partial ceria shell on the TiO_2 rutile nanopowders (TCR1). The thickness of the ceria layer is thinner than 2 nm.

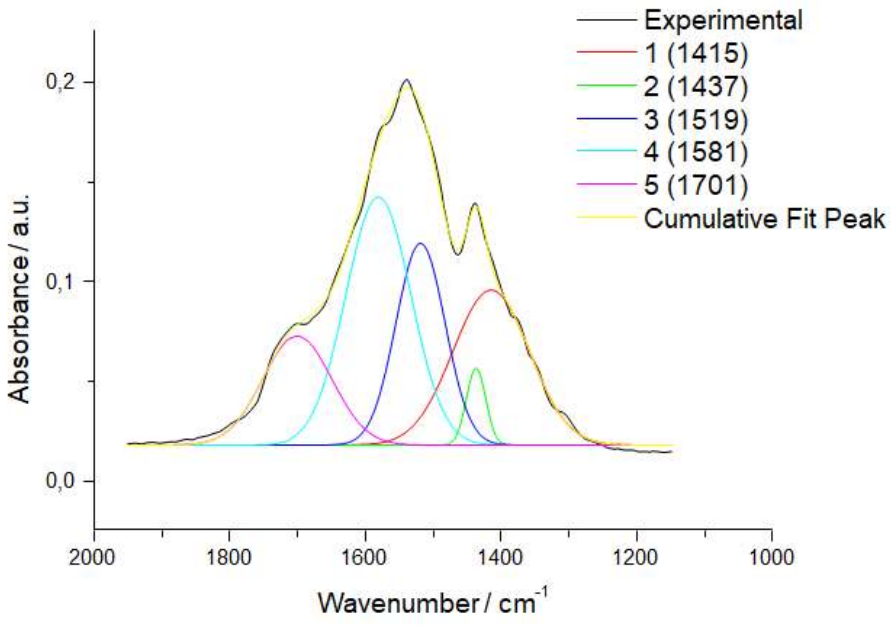

Figure S3. Peak fitting of the DRIFTS spectrum for the sample TCR1 during Ethanol TPD at 300°C in the 1150-1950 cm^{-1} region.

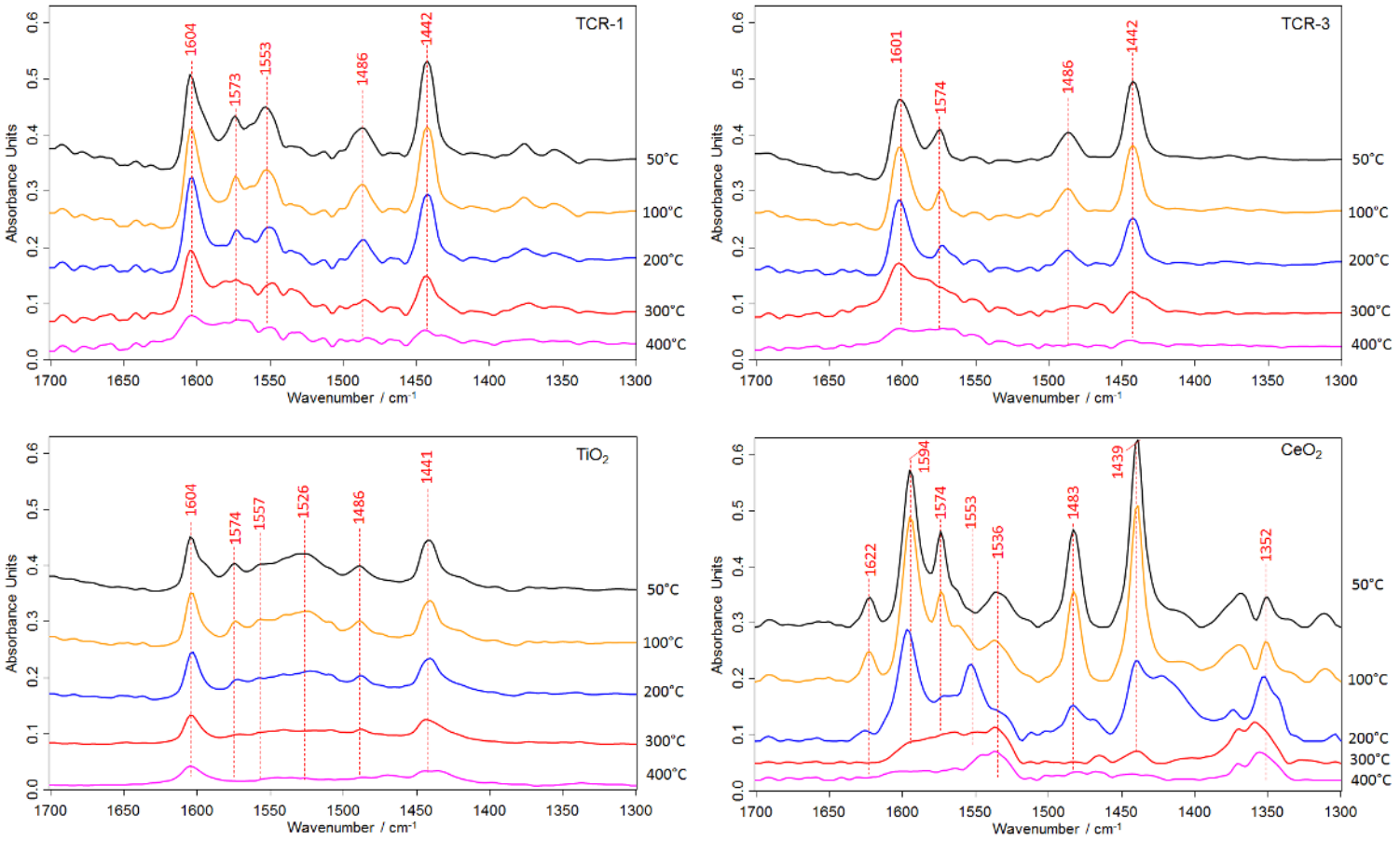

Figure S4. DRIFTS spectra after pyridine adsorption and evacuation between 50 - 400°C.

References

1. Aneggi, E., Boaro, M., Colussi, S., de Leitenburg, C. & Trovarelli, A. Ceria-Based Materials in Catalysis: Historical Perspective and Future Trends. *Handb. Phys. Chem. Rare Earths* **50,** 209–242 (2016).
2. Adachi, M. *et al.* Utilization of Nanoparticles Produced by Aqueous-Solution Methods – Formation of Acid Sites on CeO2-TiO2 Composite and 1-D TiO2 for Dye-Sensitized Solar Cells. *Smart Nanoparticles Technol.* (2012). doi:10.5772/34911
3. Wu, Z., Mann, A. K. P., Li, M. & Overbury, S. H. Spectroscopic Investigation of Surface-Dependent Acid–Base Property of Ceria Nanoshapes. *J. Phys. Chem. C* **119,** 7340–7350 (2015).
4. Reddy, B. M., Reddy, G. K. & Katta, L. Structural characterization and dehydration activity of CeO2–SiO2 and CeO2–ZrO2 mixed oxides prepared by a rapid microwave-assisted combustion synthesis method. *J. Mol. Catal. A Chem.* **319,** 52–57 (2010).
5. Ge, X., Hu, S., Sun, Q. & Shen, J. *Surface Acidity/Basicity and Catalytic Reactivity of CeO Catalysts for the Oxidative Dehydrogenation of Ethane with Carbon Dioxide to Ethylene*. *Journal of Natural Gas Chemistry* **12,** (2003).

6. Graciani, J., Plata, J. J., Sanz, J. F., Liu, P. & Rodriguez, J. A. A theoretical insight into the catalytic effect of a mixed-metal oxide at the nanometer level: The case of the highly active metal/CeOx/TiO2(110) catalysts. *J. Chem. Phys.* **132,** 104703 (2010).
7. Agnoli, S., Reeder, A. E., Senanayake, S. D., Hrbek, J. & Rodriguez, J. A. Structure and special chemical reactivity of interface-stabilized cerium oxide nanolayers on TiO_2 (110). *Nanoscale* **6,** 800–810 (2014).
8. Artiglia, L., Agnoli, S., Cristina Paganini, M., Cattelan, M. & Granozzi, G. TiO2@CeOx core-shell nanoparticles as artificial enzymes with peroxidase-like activity. *ACS Appl. Mater. Interfaces* **6,** 20130–20136 (2014).
9. Idriss, H. Ethanol Reactions over the Surfaces of Noble Metal/Cerium Oxide Catalysts. *Platin. Met. Rev.* **48,** 105–115 (2004).
10. Sheng, P.-Y., Bowmaker, G. a. & Idriss, H. The Reactions of Ethanol over Au/CeO2. *Appl. Catal. A Gen.* **261,** 171–181 (2004).
11. Yee, A., Morrison, S. J. & Idriss, H. A Study of the Reactions of Ethanol on CeO2 and Pd/CeO2 by Steady State Reactions , Temperature Programmed Desorption , and In Situ FT-IR. *J. Catal.* **186,** 279–295 (1999).
12. Nadeem, A. M., Waterhouse, G. I. N. & Idriss, H. The reactions of ethanol on TiO2 and Au/TiO2 anatase catalysts. *Catal. Today* **182,** 16–24 (2012).
13. Yee, A., Morrison, S. J. & Idriss, H. The reactions of ethanol over M / CeO 2 catalysts Evidence of carbon – carbon bond dissociation at low temperatures over Rh / CeO 2. *Catal. Today* **63,** 327–335 (2000).
14. Idriss, H. & Seebauer, E. G. Reactions of ethanol over metal oxides. *J. Mol. Catal. A Chem.* **152,** 201–212 (2000).
15. Sheng, P.-Y., Yee, A., Bowmaker, G. A. & Idriss, H. H2 Production from Ethanol over Rh–Pt/CeO2 Catalysts: The Role of Rh for the Efficient Dissociation of the Carbon–Carbon Bond. *J. Catal.* **208,** 393–403 (2002).
16. Idriss, H. & Barteau, M. A. Active sites on oxides: From single crystals to catalysts. *Adv. Catal.* **45,** 261–331 (2000).
17. Contreras, J. L. *et al.* Catalysts for H2 production using the ethanol steam reforming (a review). *Int. J. Hydrogen Energy* **39,** 18835–18853 (2014).
18. Turczyniak, S. *et al.* Surface State and Catalytic Performance of Ceria-Supported Cobalt Catalysts in the Steam Reforming of Ethanol. *ChemCatChem* **9,** 782–797 (2017).
19. Hedayati, A., Le Corre, O., Lacarrière, B. & Llorca, J. Exergetic study of catalytic steam reforming of bio-ethanol over Pd-Rh/CeO2 with hydrogen purification in a membrane reactor. *Int. J. Hydrogen Energy* **40,** 3574–3581 (2015).
20. Palma, V., Ruocco, C., Meloni, E. & Ricca, A. Oxidative steam reforming of ethanol on mesoporous silica supported PtNi/CeO2 catalysts. *Int. J. Hydrogen Energy* **2,** (2016).

21. Mondal, T., Pant, K. K. & Dalai, A. K. Catalytic oxidative steam reforming of bio-ethanol for hydrogen production over Rh promoted Ni/CeO2-ZrO2 catalyst. *Int. J. Hydrogen Energy* **40,** 2529–2544 (2015).
22. Pinzón, M. J., Alfonsoa, J. E., Olaya, J. J. & Pineda-Vargas, C. A. Annealing effect on corrosion resistance of BixTiyOz coatings. *Rev. Mex. Fis.* **62,** 450–455 (2016).
23. Agnoli, S., Reeder, A. E., Senanayake, S. D., Hrbek, J. & Rodriguez, J. A. Structure and special chemical reactivity of interface-stabilized cerium oxide nanolayers on TiO2(110). *Nanoscale* **6,** 800–810 (2014).
24. Gazsi, A., Koós, A., Bánsági, T. & Solymosi, F. Adsorption and decomposition of ethanol on supported Au catalysts. *Catal. Today* **160,** 70–78 (2011).
25. Dömök, M., Tóth, M., Raskó, J. & Erdőhelyi, A. Adsorption and reactions of ethanol and ethanol–water mixture on alumina-supported Pt catalysts. *Appl. Catal. B Environ.* **69,** 262–272 (2007).
26. Velasquez Ochoa, J., Trevisanut, C., Millet, J.-M. M., Busca, G. & Cavani, F. In Situ DRIFTS-MS Study of the Anaerobic Oxidation of Ethanol over Spinel Mixed Oxides. *J. Phys. Chem. C* **117,** 23908–23918 (2013).
27. Yee, a. A Study of Ethanol Reactions over Pt/CeO2 by Temperature-Programmed Desorption and in Situ FT-IR Spectroscopy: Evidence of Benzene Formation. *J. Catal.* **191,** 30–45 (2000).
28. Raskó, J., Hancz, a. & Erdőhelyi, a. Surface species and gas phase products in steam reforming of ethanol on TiO2 and Rh/TiO2. *Appl. Catal. A Gen.* **269,** 13–25 (2004).
29. Llorca, J., Homs, N. & Ramirez de la Piscina, P. In situ DRIFT-mass spectrometry study of the ethanol steam-reforming reaction over carbonyl-derived Co/ZnO catalysts. *J. Catal.* **227,** 556–560 (2004).
30. Rekoske, J. E. & Barteau, M. a. Competition between acetaldehyde and crotonaldehyde during adsorption and reaction on anatase and rutile titanium dioxide. *Langmuir* **15,** 2061–2070 (1999).
31. Parfitt, G. D., Ramsbotham, J. & Rochester, C. . H. An Infra-red Study of Pyridine Adsorption on Rutile Surfaces. *Trans. Faraday Soc.* **67,** 1500–1506 (1971).
32. Bezrodna, T. *et al.* Pyridine-TiO2 surface interaction as a probe for surface active centers analysis. *Appl. Surf. Sci.* **214,** 222–231 (2003).
33. Busca, G. Spectroscopic characterization of the acid properties of metal oxide catalysts. *Catal. Today* **41,** 191–206 (1998).
34. Zaki, M. I., Hasan, M. A., Al-Sagheer, F. A. & Pasupulety, L. In situ FTIR spectra of pyridine adsorbed on SiO2-Al2O3, TiO2, ZrO2 and CeO2: General considerations for the identification of acid sites on surfaces of finely divided metal oxides. *Colloids Surfaces A Physicochem. Eng. Asp.* **190,** 261–274 (2001).
35. Busca, G. The surface acidity of solid oxides and its characterization by IR spectroscopic methods. An attempt at systematization. *Phys. Chem. Chem. Phys.* **1,** 723–736 (1999).
36. Agnoli, S. Interfacial Chemistry of Low-Dimensional Systems for Applications in Nanocatalysis.

Eur. J. Inorg. Chem. **2018,** 4311–4321 (2018).